Tunable spatial–spectral phase compensation of type-I (ooe) hyperentangled photons

S. F. Hegazy[1,2] and S. S. A. Obayya[2,*]

[1]*National Institute of Laser Enhanced Sciences, Cairo University, 12613 Giza, Egypt*
[2]*Centre for Photonics and Smart Materials, Zewail City of Science and Technology, Sheikh Zayed District, 12588 Giza, Egypt*
**Corresponding author: sobayya@zewailcity.edu.eg*

Received August 25, 2014; accepted November 21, 2014;
posted December 9, 2014 (Doc. ID 221638); published February 20, 2015

The two-photon state generated by overlapping the noncollinear spontaneous parametric down conversion (SPDC) emissions of two coherently pumped type-I crystals undergoes spatial and spectral decoherence precluding the capture of high pair counts with high state fidelity. Here we present a tunable compensation method for tackling the rising state decoherence in the two degrees of freedom in the case of crystals with negative birefringence. We determine the directional-spectral phase function of the two-photon state initially and after compensation, taking into account the finite spectral width of the pump beam. Subsequently, the optimal characteristics of the compensation crystals are computed by criteria of flat phase function in spectrum and space. The results of our model are compared with measurements of some recent experiments. © 2015 Optical Society of America

OCIS codes: (270.0270) Quantum optics; (190.4410) Nonlinear optics, parametric processes.
http://dx.doi.org/10.1364/JOSAB.32.000445

1. INTRODUCTION

The process of spontaneous parametric down conversion (SPDC), in which one photon splits into two conjugate photons, is at the core of photonic entanglement. The down-converted photons, conventionally termed signal and idler, are known to memorize phase information about the pump field [1]. Based on this feature, a plethora of experiments were carried out, in which quantum interference (see [1–4]) and interferometer-based entanglement (see [5,6]) have been observed at the overlapped SPDC from separate coherently pumped nonlinear crystals.

One of the brightest two-crystal sources that does not require interferometric stability is realized by irradiating a stack of two orthogonal type-I crystals (their axes at 90° with respect to each other) by a diagonally polarized pump beam [7–16]. In this arrangement, the vertically (horizontally) polarized pump component interacting within the first (second) crystal down-converts into two horizontally (vertically) polarized signal and idler photons. The overlap of the produced noncollinear SPDC at small emission angles [17] creates hyperentangled photons (i.e., photons with simultaneous entanglement in energy, momentum, and polarization) over the entire down-conversion cones with the polarization state

$$|\psi_\phi\rangle = \frac{1}{\sqrt{2}}(|H_1H_2\rangle + e^{i\phi}|V_1V_2\rangle). \quad (1)$$

Since the crystals used in this arrangement are relatively thin, the arising transverse walk-off is negligibly small. However, because the down-conversion domain is generally birefringent and dispersive, the phase ϕ effectively varies with the angle and frequency of down-conversion emission which hurts the purity of the output state.

To obtain a high-fidelity entangled state without restricting the detection to narrow spatial–spectral windows, the phase variation needs to be manipulated by appropriate phase compensation. Altepeter *et al.* [10] could partially compensate the spatial phase variation by placing two nonlinear crystals into the signal and idler trajectories. This led to a sevenfold improvement in the spatial phase flatness which heavily enhanced the brightness of the output without sacrificing the quality. The same method has been adopted in combination with temporal compensation, while low coherence-time pump and wide collection apertures are in use [13]. A more recent technique suggests the use of a spatial phase modulator to impose spatial polarization-dependent phase differences, pixel by pixel [15].

To set up a compensation that counts for the spatial and spectral phase variations, we must determine the directional-spectral phase function of the two-photon state. One calculation approach [10,13,18] involves a number of approximations, including monochromaticity of the pump beam and SPDC radiation and symmetry of phase differences at the two down-conversion directions. Another approach considers only the first-order expansion of the phase function in a number of contributing parameters [15]. While the first approach includes unjustified approximations (led to significant mismatch between calculations and measurements), the second lacks the accuracy when higher-order phase function or wide acceptance range of frequency or direction is taken into account.

In this paper, we present a tunable compensation method for the spatial and spectral phase variations of the two-photon state generated by the noncollinear two-crystal source. Our study is confined to type-I down-conversion crystals with negative birefringence. We first determine the exact phase of the produced state as a function of frequency and angle of emission, taking into account the finite spectral width of the pump beam. Conditions for flattened phase function with respect to frequency and angle of emission are then employed to engineer the characteristics of the compensation elements. The

 © 2015 Optical Society of America

compensation profile can be broadly tuned by the tilt angles of the compensation elements. A numerical code is developed to count for the directional-spectral phase function before and after the compensation elements. The results of our model are then compared with recent experimental measurements. While, in the context of this paper, we consider the geometry of two type-I crystals, similar analysis and results apply in the case of hyperentangled photon sources with a single type-I crystal and back-reflecting mirror [19–23].

2. QUANTUM STATE OF SUPERIMPOSED SPDC LIGHT

For a nonlinear type-I domain of infinite transverse extent pumped by a normally incident classical beam of circularly symmetric Gaussian profile, the two-photon state produced by the SPDC process takes the form [24]

$$|\psi\rangle = \int \mathrm{d}K_s \mathrm{d}K_i \chi^{(2)}_{\mathrm{eff}}(w_s, w_i; w_s + w_i) A_p(w_s + w_i) \times \int_{-\infty}^{\infty}\int_{-\infty}^{\infty} \mathrm{d}x\mathrm{d}y \, \exp(-i\Delta k_T . r_T) \exp\left[-\left(\frac{r_T}{W}\right)^2\right] \times \int_0^d \mathrm{d}z \, \exp(-i\Delta k_z z)|K_s\rangle|K_i\rangle, \quad (2)$$

where K_s and K_i are the signal and idler wave vectors, $\chi^{(2)}_{\mathrm{eff}}$ is the second-order effective susceptibility, the nonlinear interaction has a volume defined by W the waist of the incident pump beam and d the crystal thickness, Δk_T and Δk_z are the transverse and longitudinal wave vector mismatches, w_s and w_i are the frequencies of the signal and idler photons, and $A_p(w_s + w_i)$ is the spectral distribution function of the pump light.

When a photon pair is generated by superimposing SPDC emissions of two coherently pumped type-I crystals (see Fig. 1), the state within spectral and spatial acceptance ranges $[\Delta w_s, \Delta w_i; \Delta\theta_s, \Delta\theta_i, \Delta\phi_s, \Delta\phi_i]$ can be expressed as

$$|\psi\rangle = C_a \int_{\Delta w_s} \mathrm{d}w_s \int_{\Delta w_i} dw_i \chi^{(2)}_{\mathrm{eff}}(w_s, w_i; w_s + w_i) A_p(w_s + w_i) \times \int_{\Delta\theta_s} \mathrm{d}\theta_s \int_{\Delta\theta_i} \mathrm{d}\theta_i \int_{\Delta\phi_s} \mathrm{d}\phi_s \int_{\Delta\phi_i} \mathrm{d}\phi_i \times \exp\left[-\left(\frac{W\Delta k_T(w_s, w_i, \theta_s, \theta_i, \phi_s, \phi_i)}{2}\right)^2\right] \times \int_0^d \mathrm{d}z \, \exp[-i\Delta k_z(w_s, w_i, \theta_s, \theta_i, \phi_s, \phi_i)z] \times \exp[i\phi_g(w_s, w_i, \theta_s, \theta_i, z)] \times \{|H\rangle_{w_s,\theta_s,\phi_s}|H\rangle_{w_i,\theta_i,\phi_i} + \exp[i\phi_o + i\phi_{\mathrm{DC}}(w_s, w_i, \theta_s, \theta_i, z)]|V\rangle_{w_s,\theta_s,\phi_s}|V\rangle_{w_i,\theta_i,\phi_i}\}, \quad (3)$$

where C_a is a normalization factor, (θ_s, θ_i) and (ϕ_s, ϕ_i) are polar and azimuthal angles of signal and idler photons outside the crystals, ϕ_o is the initial phase difference between the orthogonal pump components, ϕ_{DC} is the relative phase accumulated in the SPDC process, and ϕ_g is the global phase. Although the relative phase function ϕ_{DC} appears to depend substantially on the azimuthal angles ϕ_s and ϕ_i because of the inherent variation of refractive indices, careful analysis (details will be given in a future paper) shows that such dependence is ignorable in the case of normal pump incidence and small emission angles.

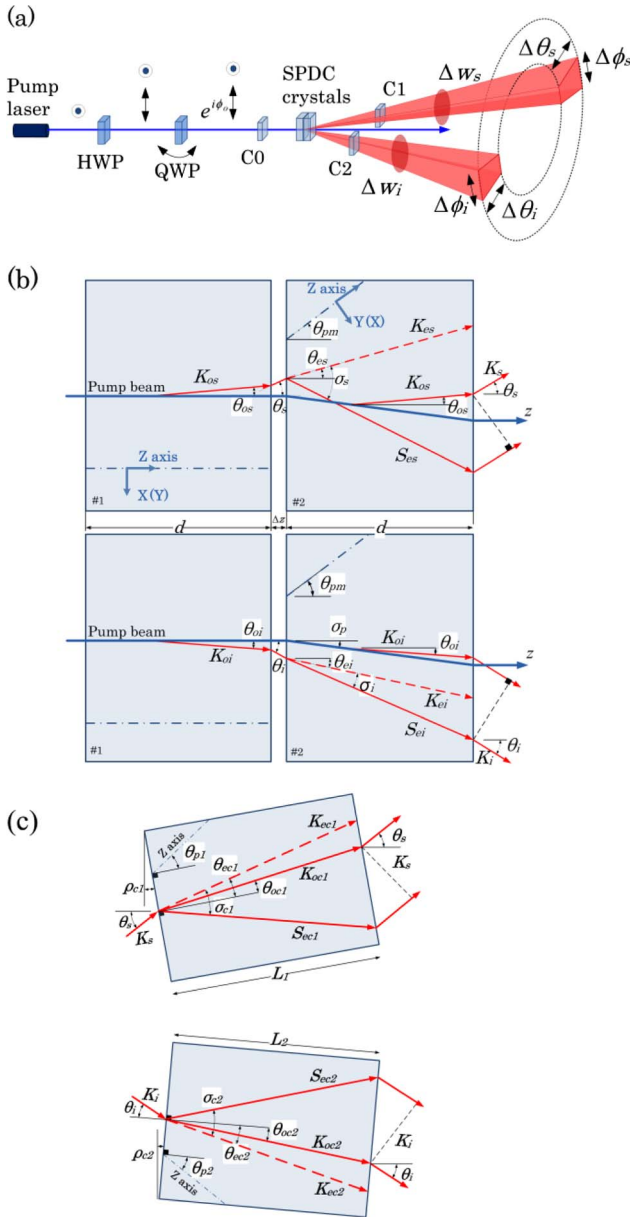

Fig. 1. (a) Outline of the noncollinear two-crystal source accompanied by the compensation elements C0, C1, and C2. The two-photon polarization state is manipulated by the quarter waveplate (QWP) and half-waveplate (HWP). Two schematics depicting Poynting and wave vectors for the signal (up) and idler (down) rays in the horizontal plane for (b) SPDC crystals and (c) post-compensation crystals C1 and C2. Note that the Z axis of the first SPDC crystal is in a plane normal to the plane of the page, while for the second SPDC crystal is in the plane of the page.

Hereinafter, the term extraordinary (ordinary) will be used to denote the field polarization with refractive index varying (constant) with the polar angle of the wave vector relative to the dielectric axis Z of uniaxial or biaxial domain. While this is the usual terminology in the case of uniaxial domain, it is applicable to the biaxial case when the wave vector lies in one of the principal dielectric planes XZ and YZ (ordinary refractive indices are thus n_y and n_x). Our analysis is confined to these two anisotropic configurations in the case of negative

birefringence (the ordinary ray is slower than the extraordinary ray).

In Eq. (3), the distribution of the relative phase ϕ_{DC} in the far field of the SPDC emission can be expressed as

$$\phi_{\mathrm{DC}}(w_s,w_i,\theta_s,\theta_i,z)=K_{op}(w_s+w_i)d+K_p(w_s+w_i)\Delta z+\phi_{\mathrm{DC}s}(w_s,\theta_s,z)+\phi_{\mathrm{DC}i}(w_i,\theta_i,z),\quad(4)$$

where $K_{op}(w_s+w_i)d$ and $K_p(w_s+w_i)\Delta z$ are the phase accumulated by the horizontal pump component in its passage through the first crystal and in the distance Δz between the two crystals. $\phi_{\mathrm{DC}s}(w_s,\theta_s,z)$ [$\phi_{\mathrm{DC}i}(w_i,\theta_i,z)$] is the phase difference between two signal (idler) photons born in the two crystals at interaction depth z. As depicted in Fig. 1, through the crystals, the extraordinary photons pass physically according to the Poynting vectors S_{en} which walk with the angle σ_n off the relevant wave vectors K_{en} $(n=s,i,p,c1,c2)$. This yields an explicit expression for the relative phase function of the form

$$\begin{aligned}\phi_{\mathrm{DC}}(w_s,w_i,\theta_s,\theta_i,z)&=K_{op}(w_s+w_i)d+K_p(w_s+w_i)\Delta z\\&-\frac{K_s(w_s)\Delta z}{\cos\theta_s}-\frac{K_s(w_s)d\sin\theta_s\cos\sigma_s}{\cos(\sigma_s-\theta_{es})\sin\theta_{es}}\\&-K_s(w_s)\sin\theta_s[d\tan(\sigma_s-\theta_{es})-\Delta z\tan\theta_s-z\tan\sigma_p]\\&-\frac{K_i(w_i)\Delta z}{\cos\theta_i}-\frac{K_i(w_i)d\sin\theta_i\cos\sigma_i}{\cos(\sigma_i+\theta_{ei})\sin\theta_{ei}}\\&+K_i(w_i)\sin\theta_i[d\tan(\sigma_i+\theta_{ei})+\Delta z\tan\theta_i-z\tan\sigma_p].\end{aligned}\quad(5)$$

It is worth observing that the phase differences at the signal and idler trajectories are not the same. This demonstrates that the symmetric-phase approximation adopted in [10,13,18] was not valid.

In Eq. (5), the transverse walk-off of the pump beam contributes to the relative-phase function by introducing dependence on the interaction depth z. This shows that, when SPDC emission is far from modes with transverse momentum conservation [for which, $K_s(w_s)\sin\theta_s=K_i(w_i)\sin\theta_i$], thicker crystals accumulate higher spatial–spectral decoherence (besides the known effect of crystal thickness on the spatial and temporal which-crystal information).

The coherent superposition of noncollinear SPDC emissions from different anisotropic domains entails pumping with a relatively wide beam to eliminate the spatial which-crystal information [7] (such requirement can be safely avoided in the collinear case [25]). The Gaussian term in Eq. (3) is thus highly selective for contribution from spatial modes with a very small transverse wave vector mismatch Δk_T. In the following, we will assume that the pump beam is wide enough [26] to offer conservation of transverse momentum as a good approximation. Accordingly, the two-photon state in Eq. (3) can be rewritten as

$$\begin{aligned}|\psi\rangle=C_b\int_{\Delta w_s}\mathrm{d}w_s\int_{\Delta w_i}\mathrm{d}w_i\chi^{(2)}_{\mathrm{eff}}(w_s,w_i;w_s+w_i)A_p(w_s+w_i)\\\times\int_{\Delta\theta_s}\mathrm{d}\theta_s\int_{\Delta\phi_s}\mathrm{d}\phi_s\times\int_0^d\mathrm{d}z\,\exp[-i\Delta k_z(w_s,w_i,\theta_s,\phi_s)z\\+i\phi_g(w_s,w_i,\theta_s,z)]\times\{|H\rangle_{w_s,\theta_s,\phi_s}|H\rangle_{w_i,\theta_i,\phi_i}\\+\exp[i\phi_o+i\phi_{\mathrm{DC}}(w_s,w_i,\theta_s)]|V\rangle_{w_s,\theta_s,\phi_s}|V\rangle_{w_i,\theta_i,\phi_i}\}.\end{aligned}\quad(6)$$

3. OPTIMAL SPATIAL–SPECTRAL PHASE COMPENSATION

After compensation, the directional-spectral relative-phase profile imposed by the compensation crystals C1 and C2 [see Fig. 1(c)], with thicknesses L_1 and L_2 and tilt angles ρ_{c1} and ρ_{c2} and of the same type as the down-conversion crystals can be written explicitly as

$$\begin{aligned}\phi_C(w_s,w_i,\theta_s)&=\phi_{C1}(w_s,\theta_s)+\phi_{C2}(w_s,w_i,\theta_s)\\&=K_s(w_s)L_1\left\{\frac{\sin\theta_s}{\sin\theta_{oc1}\cos\theta_{oc1}}-\sin(\theta_s-\rho_{c1})[\tan\theta_{oc1}\right.\\&\left.+\tan(\sigma_{c1}-\theta_{ec1})]-\frac{\sin\theta_s\cos\sigma_{c1}}{\sin\theta_{ec1}\cos(\sigma_{c1}-\theta_{ec1})}\right\}\\&+K_i(w_i)L_2\left\{\frac{\sin\theta_i(w_s,w_i,\theta_s)}{\sin\theta_{oc2}\cos\theta_{oc2}}-\sin[\theta_i(w_s,w_i,\theta_s)-\rho_{c2}]\right.\\&\left.\times[\tan\theta_{oc2}+\tan(\sigma_{c2}-\theta_{ec2})]-\frac{\sin\theta_i(w_s,w_i,\theta_s)\cos\sigma_{c2}}{\sin\theta_{ec2}\cos(\sigma_{c2}-\theta_{ec2})}\right\},\end{aligned}\quad(7)$$

where $\theta_{ocq}(\theta_{ecq})$ is the angle of the ordinary (extraordinary) wave vector $K_{ocq}(K_{ecq})$, and σ_{cq} are the walk-off angles in the two compensation crystals $(q=1,2)$. In general, the phase profile $\phi_C(w_s,w_i,\theta_s)$ can be shaped with the use of the thicknesses (L_1,L_2) and the angles $(\rho_{c1},\rho_{c2},\theta_{p1},\theta_{p2})$ of the compensation crystals to counteract the directional-spectral variations of the phase function $\phi_{\mathrm{DC}}(w_s,w_i,\theta_s)$; hence the coherence of the state is restored. Our numerical analysis demonstrates that the phase profile $\phi_C(w_s,w_i,\theta_s)$ in Eq. (7) is broadly tunable in space and frequency by means of the tilt angles of the compensation crystals (ρ_{c1},ρ_{c2}) while the crystal-cut parameters $(L_1,L_2,\theta_{p1},\theta_{p2})$ are kept fixed.

In the vicinity of its flatness, the compensated phase function ${}^C\phi_{\mathrm{DC}}=\phi_{\mathrm{DC}}+\phi_C$ becomes a slowly varying convex/concave function in its arguments. The criteria for optimal compensation can thus be expressed as

$${}^C\phi_{\mathrm{DC}}\left(w_s^0,w_i^0,\theta_s^0+\frac{\Delta\theta_s}{2}\right)={}^C\phi_{\mathrm{DC}}\left(w_s^0,w_i^0,\theta_s^0-\frac{\Delta\theta_s}{2}\right),\quad(8a)$$

$${}^C\phi_{\mathrm{DC}}\left(w_s^0+\frac{\Delta w_s}{2},w_i^0-\frac{\Delta w_i}{2},\theta_s^0\right)={}^C\phi_{\mathrm{DC}}\left(w_s^0-\frac{\Delta w_s}{2},w_i^0+\frac{\Delta w_i}{2},\theta_s^0\right),\quad(8b)$$

where the superscript "0" denotes the central directions and frequencies of the collected SPDC radiation. Here the spectral width of the pump is assumed much narrower than the acceptance ranges Δw_s and Δw_i. For optimal compensation, the six variables $(L_1,L_2,\rho_{c1},\rho_{c2},\theta_{p1},\theta_{p2})$ should take the values satisfying Eqs. (8a) and (8b). Numerically, one can find an infinite number of equivalent solutions for this problem. Four variables can thus be chosen as parameters to make the number of unknowns equal the number of equations. Under the assumption of monochromatic pump beam, and the settings $\theta_{p1}=\theta_{p2}=\theta_{pm}$ and $\rho_{c1}=\rho_{c2}=0°$, the above criteria can be reduced to

Table 1. Simulation Results for Some Previous Two-Crystal Setups

Publication	Angular Phase Slopes		Optimal Thicknesses of Compensation Crystals (μm)		Phase Range over (1°, 30 nm) (deg.)	
	Signal	Idler	L_1	L_2	Before	After
[7,10]	−185.9	543.2	302.2	297.1	400.2°	24.2°
[8]	−62.8	160.8	58.2	56.8	111.1°	11.5°
[9]	−32.0	66.8	36.5	36.1	37.5°	3.0°
[15] (0.5 mm crystals)	−114.4	381.7	284.1	280.9	296.4°	15.6°
[13] (BBO crystals)	−127.5	468.4	363.0	359.0	380.5°	18.9°
[14]	−44.0	759.2	773.9	766.1	846.8°	28.0°

$$\phi_{\mathrm{DC}}\left(w_s^0,\theta_s^0-\frac{\Delta\theta_s}{2}\right)-\phi_{\mathrm{DC}}\left(w_s^0,\theta_s^0+\frac{\Delta\theta_s}{2}\right)$$
$$=(L_1+L_2)\left[\Phi_{C1}\left(w_s^0,\theta_s^0+\frac{\Delta\theta_s}{2}\right)-\Phi_{C1}\left(w_s^0,\theta_s^0-\frac{\Delta\theta_s}{2}\right)\right], \quad (9a)$$

$$\phi_{\mathrm{DC}}\left(w_s^0+\frac{\Delta w_s}{2},\theta_s^0\right)-\phi_{\mathrm{DC}}\left(w_s^0-\frac{\Delta w_s}{2},\theta_s^0\right)$$
$$=L_1\left[\Phi_{C1}\left(w_s^0-\frac{\Delta w_s}{2},\theta_s^0\right)-\Phi_{C1}\left(w_s^0+\frac{\Delta w_s}{2},\theta_s^0\right)\right]$$
$$+L_2\left[\Phi_{C2}\left(w_s^0-\frac{\Delta w_s}{2},\theta_s^0\right)-\Phi_{C2}\left(w_s^0+\frac{\Delta w_s}{2},\theta_s^0\right)\right], \quad (9b)$$

where $\Phi_{C1}=\phi_{C1}/L_1$ and $\Phi_{C2}=\phi_{C2}/L_2$.

4. RESULTS AND DISCUSSION

We have developed a numerical code (available on our website [27]) to calculate the phase functions, the optimal characteristics of compensation elements, and other parameters associated with the problem. We detail in Table 1 the results of phase calculations for a number of two-crystal setups, assuming irradiation by a monochromatic pump beam. These results are accompanied by the optimal thicknesses of compensation crystals in each case as obtained by Eqs. (9a) and (9b). In each case, we assume that the biphoton flux is collected over many spatial modes.

Let us discuss one of the cases in Table 1 in detail. In [7,10], Fig. 2 depicts linear increase in the spatial and spectral slopes of the relative-phase function as the two down-conversion crystals are shifted farther from each other. Any desired two-photon state can then be captured only along specific spatial–spectral modes of the noncollinear two-crystal radiation (in agreement with [28,29]).

The angular phase slopes in Table 1 correspond to spatial slopes of about −8.85°/mm (signal) and 25.86°/mm (idler) at a transverse plane, 120 cm from the down-conversion crystals. The spatial slope of the relative-phase function is thus 17.01°/mm, as depicted in Fig. 3(a). This perfectly agrees with the slope value determined experimentally by taking complete state tomography at different points in the transverse plane (17°/mm in [10]).

In this case, using the compensation setup in Table 1, our calculation model predicts a relative-phase range of about 24.0° over angular-spectral ranges (1°, 30 nm) [see Fig. 3(b)]. Any deviation from the optimal (L_1+L_2) value determined by Eq. (9a) directly boosts the spatial phase variation. For instance, let us consider the compensation realized by Altepeter *et al.* using two 245 μm crystals. The residual phase slope, calculated by our code for this suboptimal setup is ≈3.1°/mm, on average [see Fig. 3(c)]. This excellently agrees with the slope ≈3.0°/mm measured experimentally in [10].

On the other hand, the higher the deviation from the ratio (L_1/L_2) obtained by Eqs. (9a) and (9b), the more the phase variation in the frequency dimension. For example, while a 599 μm compensation crystal at one arm eliminates the spatial phase variation [satisfying Eq. (8a)], it increases the spectral phase gradient, as depicted in Fig. 3(d). The above discussion can be generalized to all other cases in Table 1.

Moreover, the increment of the inter-crystal distance Δz that corresponds to a relative-phase shift φ can be given by Eq. (5) as

$$\Delta z_\varphi \cong \frac{\varphi}{K_p(w_s+w_i)-\frac{K_s(w_s)}{\cos\theta_s}-\frac{K_i(w_i)}{\cos\theta_i}}. \quad (10)$$

The same relation applies to hyperentanglement setups with single type-I crystal and back-reflecting mirror [19–23] (except for a factor of $\frac{1}{2}$ because of the double pass). For a degenerate down-conversion with wavelength 727.6 nm and emission angle 3.3°, we determine $\Delta z_\pi \cong 55.5$ μm which agrees with the experimental measurements in [19] ($\Delta z_\pi = 55$ μm).

It should be noted that, by virtue of the tilt angles ρ_{c1} and ρ_{c2}, the phase profile imposed by the compensation crystals is broadly tunable in both frequency and angle of emission. For example, as demonstrated by numerical simulations, the suboptimal compensation using two 245 μm crystals can be made optimal by tilting the compensation crystals with $\rho_{c1}=25.6°$

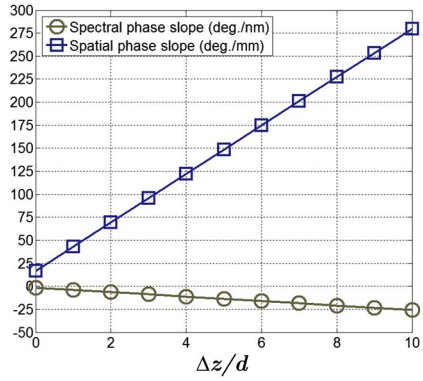

Fig. 2. Average spatial and spectral slopes of the relative-phase function $\phi_{\mathrm{DC}}(w_s,w_i,\theta_s)$ versus the ratio of inter-crystal distance Δz to the crystal thickness d. The average slopes are calculated at 120 cm from BBO crystals over an angular-spectral window (1°, 30 nm) centered at the degenerate frequency and central emission angle for $\lambda_p=351.1$ nm, $\theta_{pm}=33.9°$, and $d=0.59$ mm.

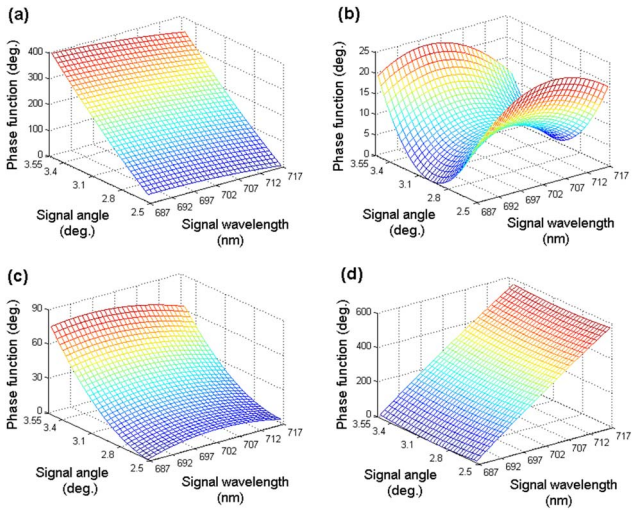

Fig. 3. (a) Predicted relative-phase function $\phi_{\mathrm{DC}}(w_s, w_i, \theta_s)$ for the two-crystal arrangement in [7,10]. (b) The relative-phase function after the optimal compensation derived by the criteria for Eqs. (9a) and (9b). The phase range is about 24.0° over a centralized (1°, 30 nm) angular-spectral window. (c) The relative-phase function behind two 245-μm crystals. A phase range of about 76.7° with an average spatial slope ≈3.1°/mm is predicted. (d) The compensated relative-phase function when a 599 μm crystal is placed at the signal or the idler arms. (An overall phase offset has been suppressed in all figures.)

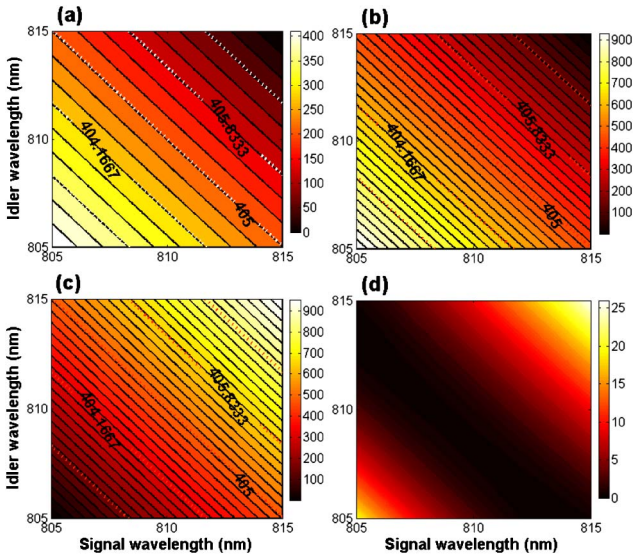

Fig. 4. Spectral relative phase function $\phi_{\mathrm{DC}}(w_s, w_i, \theta_s^p)$ for the two-crystal arrangement in [13]. The bold-dotted lines highlight the corresponding values of the pump wavelength. Here the emission angle θ_s^p takes value determined by perfect phase matching in longitudinal and transverse directions, while the pump wavelength is considered broadened between 402.5 nm (left-bottom corner) and 407.5 nm (up-right corner). (a) Spectral relative phase function behind the SPDC crystals (b) Spectral relative phase function behind the optimal spatial–spectral compensation setup in Table 1. (c) Spectral phase profile imposed by a 575 μm BBO crystal with a 90° cut angle and 0° tilt angle placed before the SPDC crystals. (d) Compensated spectral relative-phase function. (In all figures, each outlined level of the phase contour is 25°, and an overall phase offset has been suppressed.)

and $\rho_{c2} = 25.0°$. Equations (8a) and (8b) are thus satisfied, and the compensated phase function becomes similar to the one in Fig. 3(b) with a range of about 24.0° over (1°, 30 nm) window. This shift toward tunable phase compensation is substantially useful to realize optimal compensation for the nondegenerate SPDC arrangements using compensation elements satisfying Eqs. (9a) and (9b) in the degenerate case.

In the discussion above, we describe the optimal spatial–spectral phase compensation under the assumption of monochromatic pump beam. Figure 4(a) shows the spectral phase function for the two-crystal arrangement in [13] when a finite pump line width is taken into account and perfect phase matching is assumed in longitudinal and transverse directions. One can observe that, over wide ranges of signal and idler wavelengths, the variations of the phase mainly come with the pump wavelength. It seems as though the perfect phase matching with underlying conservation of energy and momentum also offers conservation of relative phase all over the emission directions.

The complete phase picture can be visualized as follows. The central spatial–spectral SPDC modes determined by perfect phase matching conditions have fixed relative phase over space and spectrum when monochromatic pump beam is considered. Because of the loose phase-matching condition in the longitudinal direction, there exist spatial–spectral SPDC modes around each central mode which receive relative-phase value, deviated from the phase of the central modes [as in Fig. 3(a)]. When a broad-bandwidth pump is used, the relative phase of the central spatial–spectral SPDC modes exhibits significant dependence on the pump wavelength. This consequently affects the phase of the noncentral spatial–spectral modes.

To compensate for the spectral phase gradient in the case of a broad-bandwidth pump, one might extend the criteria in Eqs. (8a) and (8b) by involving another equality to address the weakly related signal and idler wavelengths. Values for three compensation variables, rather than two, are thus determined by solving the three equations together. Another way is to supplement the compensation setup satisfying Eqs. (8a) and (8b) by an additional crystal placed in front of the SPDC crystals. The spectral phase profile of the pre-compensation crystal counteracts the spectral phase gradient of the SPDC crystals and post-compensation crystals, as depicted in Figs. 4(b)–4(d). One unknown variable of the pre-compensation crystal (either thickness, cut angle, or tilt angle) thus can be determined by solving the equality

$$
\begin{aligned}
&{}^{C}\phi_{\mathrm{DC}}\left[w_s^0 + \frac{\Delta w_s}{2}, w_i^0 + \frac{\Delta w_i}{2}, \theta_s^p(w_s, w_i)\right] \\
&\quad = {}^{C}\phi_{\mathrm{DC}}\left[w_s^0 - \frac{\Delta w_s}{2}, w_i^0 - \frac{\Delta w_i}{2}, \theta_s^p(w_s, w_i)\right], \qquad (11)
\end{aligned}
$$

where $\theta_s^p(w_s, w_i)$ is the emission angle of a signal photon in the case of perfect phase matching and ${}^{C}\phi_{\mathrm{DC}}$ is the final compensated phase function. Remarkably, any combination of compensation variables satisfying (11) is found also to compensate entirely for the temporal walk-off accumulated over the SPDC crystals and post-compensation crystals.

5. CONCLUSION

The spatial–spectral phase variation of the two-photon state generated by the noncollinear two-crystal SPDC emission limits its output efficiency. In this paper, an experimentally

convenient method for tunable phase compensation has been presented in the case of negative birefringent domains. We have determined the exact directional-spectral relative phase function of the output state. We have then employed optimal flatness criteria for the compensated phase over frequency and direction to engineer the compensation elements. We have also studied the dependence on the distance separating the down-conversion crystals. Our theoretical results, supported by numerical simulations, perfectly agree with preceding experimental measurements.

REFERENCES AND NOTES

1. Z. Y. Ou, L. J. Wang, X. Y. Zou, and L. Mandel, "Evidence for phase memory in two-photon down conversion through entanglement with the vacuum," Phys. Rev. A **41**, 566–568 (1990).
2. D. N. Klyshko, "Combined EPR and two-slit experiments: interference of advanced waves," Phys. Lett. A **132**, 299–304 (1988).
3. X. Y. Zou, L. J. Wang, and L. Mandel, "Induced coherence and indistinguishability in optical interference," Phys. Rev. Lett. **67**, 318–321 (1991).
4. A. V. Burlakov, M. V. Chekhova, D. N. Klyshko, S. P. Kulik, A. N. Penin, Y. H. Shih, and D. V. Strekalov, "Interference effects in spontaneous two-photon parametric scattering from two macroscopic regions," Phys. Rev. A **56**, 3214–3225 (1997).
5. A. V. Burlakov, M. V. Chekhova, O. A. Karabutova, D. N. Klyshko, and S. P. Kulik, "Polarization state of a biphoton: quantum ternary logic," Phys. Rev. A **60**, R4209–R4212 (1999).
6. Y. H. Kim, M. V. Chekhova, S. P. Kulik, M. H. Rubin, and Y. Shih, "Interferometric Bell-state preparation using femtosecond-pulse-pumped spontaneous parametric down-conversion," Phys. Rev. A **63**, 062301 (2001).
7. P. G. Kwiat, E. Waks, A. G. White, I. Appelbaum, and P. H. Eberhard, "Ultrabright source of polarization entangled photons," Phys. Rev. A **60**, R773–R776 (1999).
8. Y. Nambu, K. Usami, Y. Tsuda, K. Matsumoto, and K. Nakamura, "Generation of polarization-entangled photon pairs in a cascade of two type-I crystals pumped by femtosecond pulses," Phys. Rev. A **66**, 033816 (2002).
9. D. Dehlinger and M. W. Mitchell, "Entangled photons, nonlocality, and Bell inequalities in the undergraduate laboratory," Am. J. Phys. **70**, 903–910 (2002).
10. J. B. Altepeter, E. R. Jeffrey, and P. G. Kwiat, "Phase-compensated ultra-bright source of entangled photons," Opt. Express **13**, 8951–8959 (2005).
11. A. Gogo, W. D. Snyder, and M. Beck, "Comparing quantum and classical correlations in a quantum eraser," Phys. Rev. A **71**, 052103 (2005).
12. S. Cialdi, F. Castelli, and M. G. A. Paris, "Properties of entangled photon pairs generated by a CW laser with small coherence time: theory and experiment," J. Mod. Opt. **56**, 215–225 (2009).
13. R. Rangarajan, M. Goggin, and P. G. Kwiat, "Optimizing type-I polarization-entangled photons," Opt. Express **17**, 18921–18933 (2009).
14. S. F. Hegazy, M. S. Mansour, and L. El-Nadi, "Enhanced type-I polarization-entangled photons using CW-diode laser," in *Modern Trends in Physics Research—Proceedings of the 4th International Conference on MTPR-10* (World Scientific, 2010), pp. 211–220.
15. S. Cialdi, D. Brivio, and M. G. A. Paris, "Programmable purification of type-I polarization-entanglement," Appl. Phys. Lett. **97**, 041108 (2010).
16. S. Straupe and S. Kulik, "The problem of preparing entangled pairs of polarization qubits in the frequency-nondegenerate regime," J. Exp. Theor. Phys. **110**, 185–192 (2010).
17. A. Migdall, "Polarization directions of noncollinear phase-matched optical parametric downconversion output," J. Opt. Soc. Am. B **14**, 1093–1098 (1997).
18. G. M. Akselrod, J. B. Altepeter, E. R. Jeffrey, and P. G. Kwiat, "Phase-compensated ultra-bright source of entangled photons: erratum," Opt. Express **15**, 5260–5261 (2007).
19. G. Giorgi, G. Di Nepi, P. Mataloni, and F. De Martini, "A high brightness parametric source of entangled photon states," Laser Phys. **13**, 350–354 (2003).
20. C. Cinelli, G. Di Nepi, F. De Martini, M. Barbieri, and P. Mataloni, "Parametric source of two-photon states with a tunable degree of entanglement and mixing: experimental preparation of Werner states and maximally entangled mixed states," Phys. Rev. A **70**, 022321 (2004).
21. M. Barbieri, C. Cinelli, P. Mataloni, and F. De Martini, "Polarization-momentum hyperentangled states: realization and characterization," Phys. Rev. A **72**, 052110 (2005).
22. M. Barbieri, F. De Martini, P. Mataloni, G. Vallone, and A. Cabello, "Enhancing the violation of the Einstein-Podolsky-Rosen local realism by quantum hyperentanglement," Phys. Rev. Lett. **97**, 140407 (2006).
23. M. Barbieri, G. Vallone, P. Mataloni, and F. De Martini, "Complete and deterministic discrimination of polarization Bell states assisted by momentum entanglement," Phys. Rev. A **75**, 042317 (2007).
24. A. Joobeur, B. E. A. Saleh, T. S. Larchuk, and M. C. Teich, "Coherence properties of entangled light beams generated by parametric down-conversion: theory and experiment," Phys. Rev. A **53**, 4360–4371 (1996).
25. P. Trojek and H. Weinfurter, "Generation of quantum-correlated and/or polarization entangled photon pairs with unequal wavelengths," U.S. patent 8,222,623 B2 (July 17, 2012).
26. A plausible condition in this case is $W \gg 2/\Delta k_T$ for $\Delta k_T \ll k_x, k_y$.
27. http://www.zewailcity.edu.eg/research-institutes/cpsm/.
28. T. J. Herzog, P. G. Kwiat, H. Weinfurter, and A. Zeilinger, "Complementarity and the quantum eraser," Phys. Rev. Lett. **75**, 3034–3037 (1995).
29. T. J. Herzog, J. G. Rarity, H. Weinfurter, and A. Zeilinger, "Frustrated two-photon creation via interference," Phys. Rev. Lett. **72**, 629–632 (1994).